JOURNAL OF APPLIED ELECTROCHEMISTRY 8 (1978) 491–501

The current distribution and shape change of zinc electrodes in secondary silver-zinc cells

S.-P. POA, C. H. WU

Department of Industrial Chemistry, National Tsing Hua University, Hsin-Chu, Taiwan, ROC

Received 11 November 1977

The current and potential distributions of zinc electrodes in secondary zinc–silver oxide cells during cycling were studied using a sectioned electrode technique. The shape change occurring in zinc electrodes resulting from cell cycling was examined. The zinc electrodes used for this study were of a conventional type of design and were fabricated by a slurry paste method. The positive electrodes used were sectioned silver oxide electrodes, each of which comprised nine sections of sintered silver plates. The results indicate that, by adding a layer of non-woven fabric treated with Fe_2O_3 to the edge sections of the electrode separator system, the uniformity of the current and potential distributions on the zinc electrodes during cell cycling can be improved, and the zinc electrode shape change resulting from cell cycling can be effectively suppressed.

1. Introduction

This work is a continuation of an earlier study [1] on zinc electrode shape change resulting from cell cycling. The purposes of this study were to examine the current and potential distribution on zinc electrodes in secondary zinc–silver oxide cells during cycling, and to test the effect of a modification of the electrode separator system on the current and potential distribution patterns, and on the alleviation of zinc electrode shape change.

The major problem in the study of zinc electrode shape change has been the growth of zinc dendrites on recharging. Consequently, the morphology of zinc electrodeposited from aqueous alkaline solution has been the subject of extensive studies [2–9]. It is necessary to be able to define the modes of mass transfer precisely in order to make any quantitative predictions about the behaviour of the zinc electrode. This problem is linked to the distribution of current and potential on the electrodes. Breiter [10] studied the dissolution and passivation of vertical, porous zinc electrodes in solutions of 6 M KOH–0·25 M ZnO using a potential-sweep technique. Nagy and Bockris [11] discharged the porous zinc electrodes galvanostatically and studied the morphology of the film formed with a scanning electron microscope. The current distribution in the electrode was determined by chemical analysis of microslices of the electrode after discharge. In order to fit the current distribution observed to that expected, they postulated a thin, highly-resistive film as being simultaneously present on the zinc surface. Elsdale *et al.* [12] suggested that the film is formed by a dissolution–precipitation mechanism and that the major component of the electrode polarization is due to the ohmic resistance of this film. Several groups of workers [13–18] have studied the passivation of zinc in concentrated alkali using the constant-current technique. McBreen [19] has investigated the mechanism of zinc electrode shape change by monitoring the current and potential distribution patterns of zinc electrodes during cycling.

2. Experimental

The materials, chemicals, and the zinc electrode preparation method used for this study were the same as those described previously [1].

2.1. *Preparation of the sectioned silver oxide electrode*

The positive (silver oxide) electrode used for this study comprised nine sections of sintered silver plates. The essential procedure in the preparation

of sectioned silver electrodes was as follows. Each section of the sintered silver plates was made by pasting an electrode mixture (1·0 g AgO powder + 0·2 ml of 0·5 wt% CMC solution) onto the silver grid cut from the expanded silver screen. The pasted section was dried at 75–80° C for about 30 min and was then put in the oven for sintering by preheating first at 200° C for 20 min, the temperature was then raised to 450° C and kept at this temperature for about 30 min. After sintering, the section was pressed at 100 kg cm^{-2} and electroformed in 5% KOH solution against a nickel dummy electrode at a rate of 2 mA cm^{-2} for about 22 hours. It was then washed with distilled water to remove any KOH, and dried. The final plate dimensions were 2·0 x 2·0 x 0·5 cm. After a silver tab had been spot-welded onto each section, the nine-section plates were arranged on an acrylic plastic plate with dimensions of 6·5 x 6·5 x 0·4 cm.

2.2. *Test cell system*

The reference electrode compartments were 0·4 cm diameter holes drilled vertically in an acrylic plastic block (6·8 x 9·0 x 2·5 cm). The reference electrode capillaries were 0·1 cm diameter holes from the reference compartment to one face of the acrylic block. These holes were drilled at a 20° angle to the normal of the block face. These compartments were used for the preparation of the array of Hg/HgO electrodes.

A schematic diagram of the test cell assembly and circuitry is shown in Fig. 1. The test cell consisted of a zinc electrode, a separator system, a sectioned silver oxide electrode, and an array of Hg/HgO reference electrodes. Two cells (Cell 1 and Cell 2) were used in this study. The electrode separator system for Cell 1 consisted of one layer of Webril E1452 non-woven polypropylene, three layers of RAI IC 40/100 radiation-grafted cellophane membrane, one layer of no. 572 filter paper

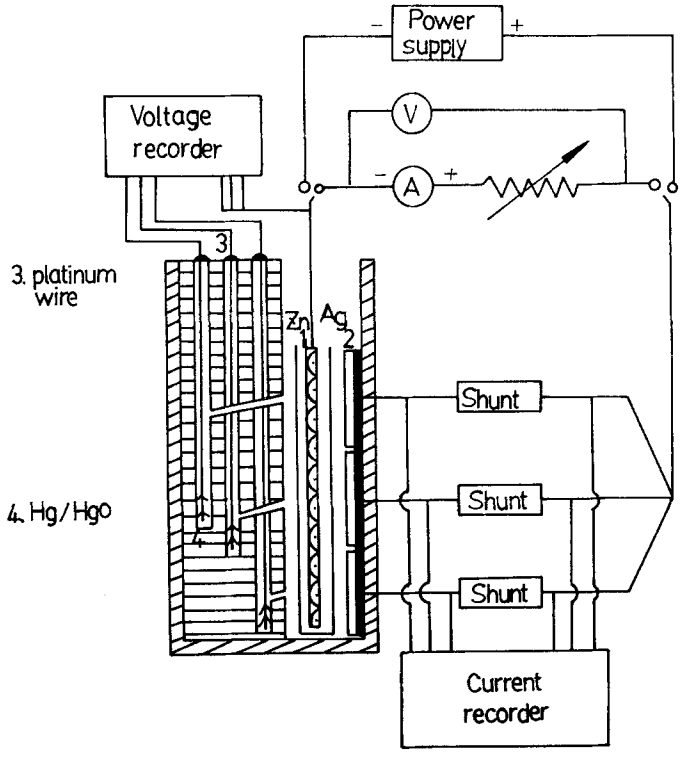

Fig. 1. Schematic diagram of test cell assembly and electrical circuit.

and one layer of S-950-CLS 3463 Viskon separator which was placed on the silver electrode side of the separator system. The electrode separator system for Cell 2 consisted of an additional layer of Webril E1452 non-woven polypropylene treated with Fe_2O_3, as described previously [1].

2.3. *Experimental procedure*

After the test cell had been filled with 30 ml of electrolyte [40% KOH solution + 60 mg ZnO $(ml\ KOH)^{-1}$] and soaked for 24 hours, the cycling test was started. For Cell 1, the initial 15 test cycles were done by discharging at 1·0 A to 1·30 V (the terminating cut-off voltage was set at 1·30 V), and charging at 0·3 A to 2·10 V. Cycles 16–38 were carried out by discharging the cell at 1·0 A to 1·20 V, and charging at 0·2 A to 2·0 V.

For Cell 2, the initial 39 test cycles were carried out by discharging the cell at 1·0 A to 1·20 V, and charging at 0·5 A to 2·10 V. Cycles 40–60 were carried out by discharging at 2·0 A to 1·2 V, and charging at 1·0 A to 2·10 V.

During cycling, current distribution was determined by monitoring the currents to the various sections of the silver oxide electrode which, in turn, were monitored by measuring the voltage across the shunts (resistance: 0·05 Ω each) on the recorders.

Charge and discharge curves were displayed using one Gould Brush 220 and two Linear Model 232 recorders. Constant currents and potentials were supplied by conventional regulated power supplies.

After cycling tests, the zinc electrode was removed from the test cell assembly in the charged condition and was examined for general patterns of shape change using a Cambridge JUS-3 scanning electron microscope. The zinc electrode was then washed thoroughly with distilled water to remove the electrolyte. After being dried at about 50° C, the zinc electrode was cut into nine sections of equal size (2·0 × 2·0 cm) which were marked according to their relative positions and numbered 1–9 (as shown in Figs. 17 and 18). The thickness and weight of each section were measured carefully to obtain accurate quantitative data of electrode shape change.

3. Results

The nine sections of each electrode were divided into the following three groups: Sections 1, 5, and 9; Sections 2, 6, and 7; and Sections 3, 4, and 8. The current and potential distributions of only one group of the sections were recorded at a predetermined cycle when recording was to be made, and the three groups were recorded in turn.

The current and potential distributions of different sections of the zinc electrodes of Cell 1 and Cell 2 at different stages of cycling are shown in Figs. 2–7 and Figs. 8–16, respectively.

3.1. *Current and potential distribution of the zinc electrode of Cell 1*

For Cell 1, in the early stages of cycling (Cycles 1–3, as shown in Figs. 2–4), there was a large vari-

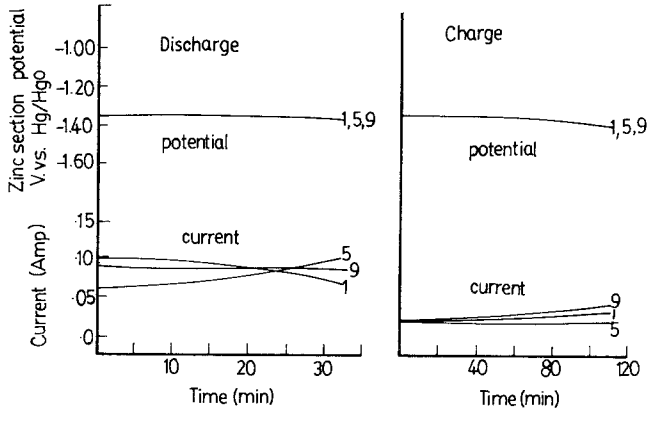

Fig. 2. Current and potential distribution of Sections 1, 5 and 9 of the zinc electrode for Cell 1 at Cycle 1.

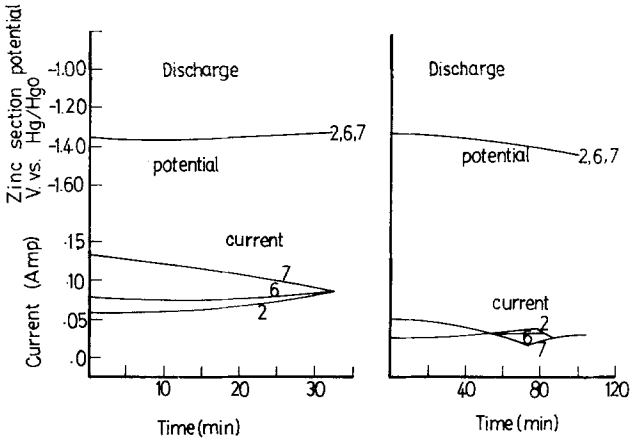

Fig. 3. Current and potential distribution of Sections 2, 6 and 7 of the zinc electrode for Cell 1 at Cycle 2.

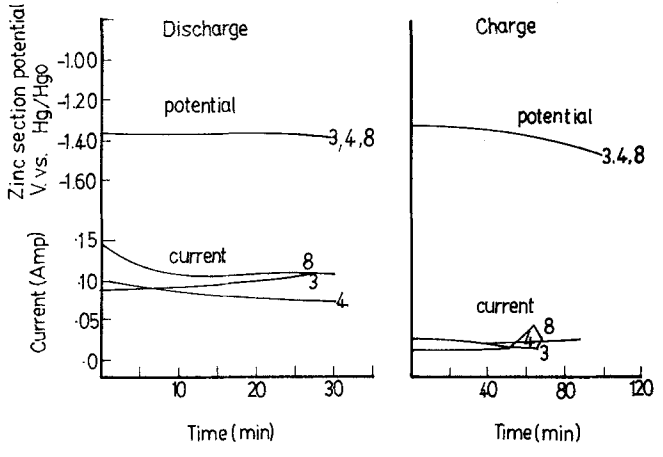

Fig. 4. Current and potential distribution of Sections 3, 4 and 8 of the zinc electrode for Cell 1 at Cycle 3.

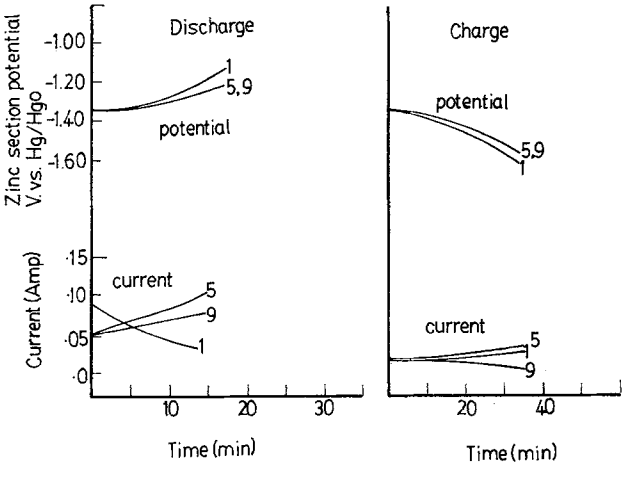

Fig. 5. Current and potential distribution of Sections 1, 5 and 9 of the zinc electrode for Cell 1 at Cycle 34.

ation in the current distribution at the beginning of discharge; the edge sections (Sections 1, 7 and 8) operated at higher partial currents than those of the central sections. This variation of current distribution on discharge diminished with time. The variation in current distribution at the beginning of charging was very small, the currents tended to diverge with time, and then finally converged rapidly to a uniform current distribution when the cell was charged to a higher potential. It is shown that the potential distribution was uniform on both discharge and charge in the early stages of cycling. In the intermediate stages of cycling of Cell 1 (Cycles 13–15), the pattern of current distribution was similar to that of the early stages of cycling; the current density on the edge sections was higher than that on the central sections of the electrode on discharge. However, the potential distribution showed a significant variation at the end of both discharging and charging; Sections 1, 4 and 7 polarized more than any other sections of the electrode. In the later stages of cycling (Cycles 25–27), the discharge current on the top edge sections (Sections 1, 2 and 7) decreased, whereas the discharge current on the middle and lower sections (Sections 3, 5 and 6) increased. Towards the end of cycling (Cycles 34–36 as shown in Figs. 5–7), this trend of variation in current distribution continued to develop, and the extent of non-uniformity in current distribution over the electrode surface continued to increase.

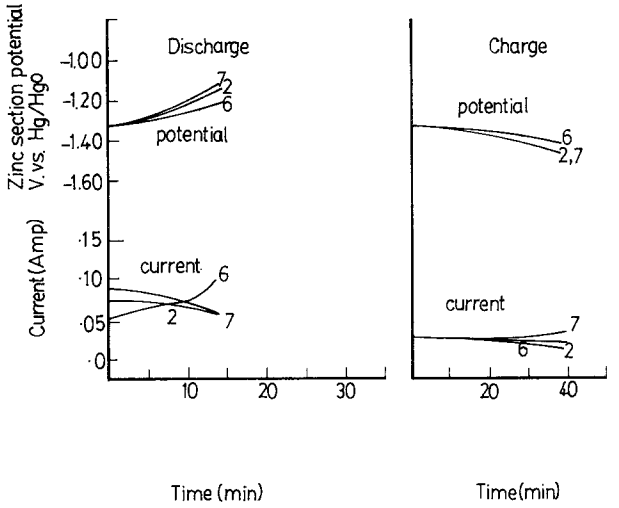

Fig. 6. Current and potential distribution of Sections 2, 6 and 7 of the zinc electrode for Cell 1 at Cycle 35.

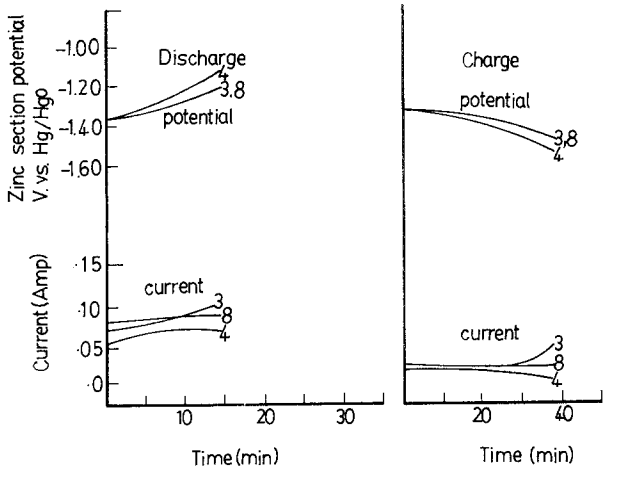

Fig. 7. Current and potential distribution of Sections 3, 4 and 8 of the zinc electrode for Cell 1 at Cycle 36.

3.2. *Current and potential distribution of the zinc electrode of Cell 2*

The patterns of current and potential distribution on different sections of the zinc electrode for Cell 2 at different stages of cycling, as shown in Figs. 8–16, showed a significant improvement over those of Cell 1. In the early stages of cycling (Cycles 1–3, as shown in Figs. 8–10), the variation in current distribution at the beginning of discharge was not so large as that of Cell 1. The current distribution was more uniform and tended to converge with time during discharge. At the beginning of charge, the variation in current distribution over the electrode surface was small. The currents of different sections then diverged with time of charging, and finally converged rapidly to a uniform current distribution. The current distribution on the zinc electrode of Cell 2 at Cycles 16–18 (as shown in Figs. 11–13) followed the same trend during both discharging and charging, but the potential distribution at the end of both processes started to vary. In the intermediate stages of cycling (Cycles 31–33), the pattern of current distribution over the surface of the electrode on discharge was similar to that observed in the early stages of cycling. The current distribution diverged with time initially and then converged rapidly to a uniform distribution. It can be observed that the period of time for the occurrence of such a transition decreased continuously with increase of cycle number. After 40 cycles, the rate of discharge and the rate of charge of Cell 2 were raised to 2·0 A and 1·0 A, respectively, for

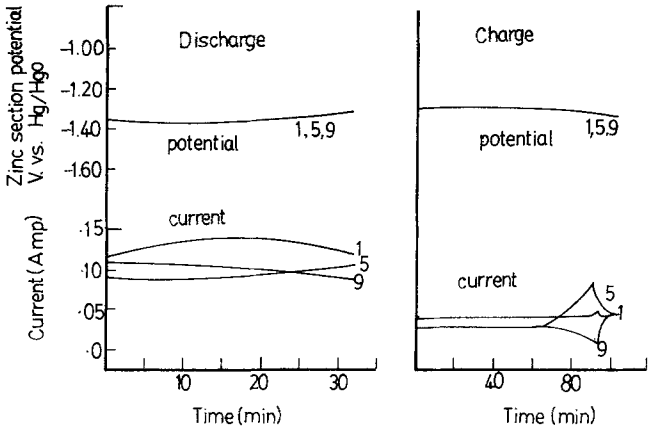

Fig. 8. Current and potential distribution of Sections 1, 5 and 9 of the zinc electrode for Cell 2 at Cycle 1.

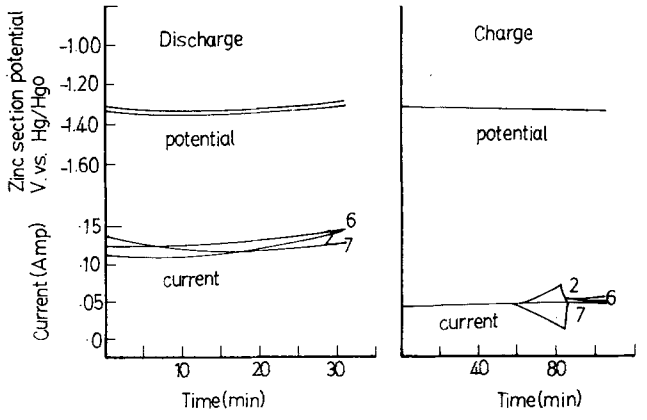

Fig. 9. Current and potential distribution of Sections 2, 6 and 7 of the zinc electrode for Cell 2 at Cycle 2.

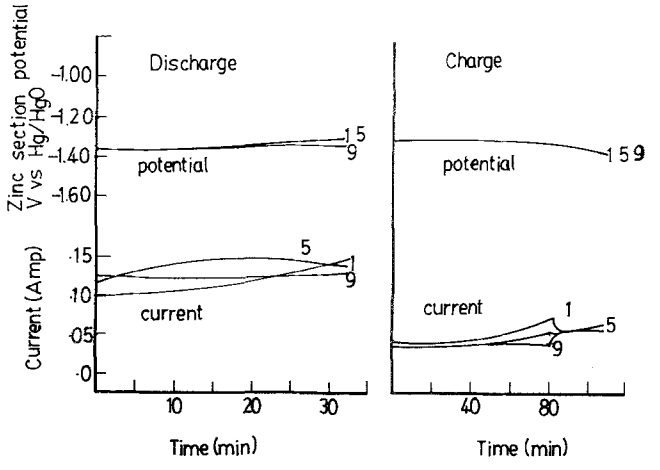

Fig. 10. Current and potential distribution of Sections 3, 4 and 8 of the zinc electrode for Cell 2 at Cycle 3.

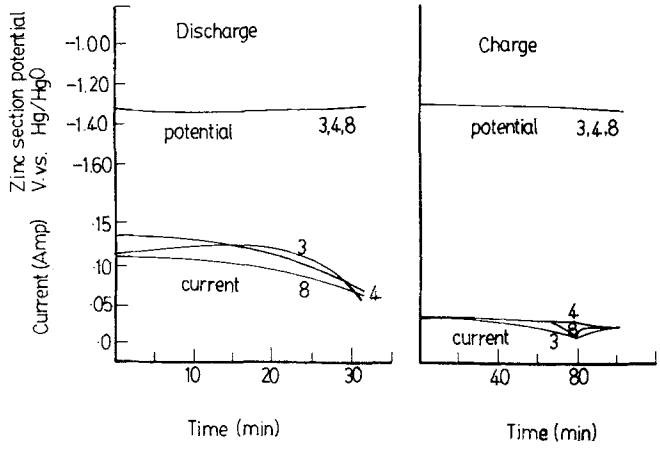

Fig. 11. Current and potential distribution of Sections 1, 5 and 9 of the zinc electrode for Cell 2 at Cycle 16.

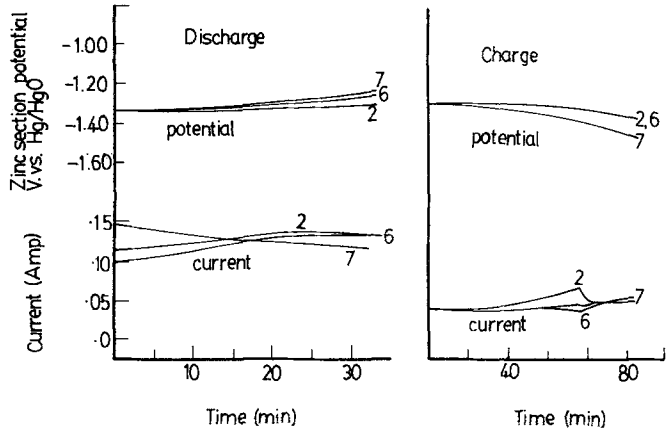

Fig. 12. Current and potential distribution of Sections 2, 6 and 7 of the zinc electrode for Cell 2 at Cycle 17.

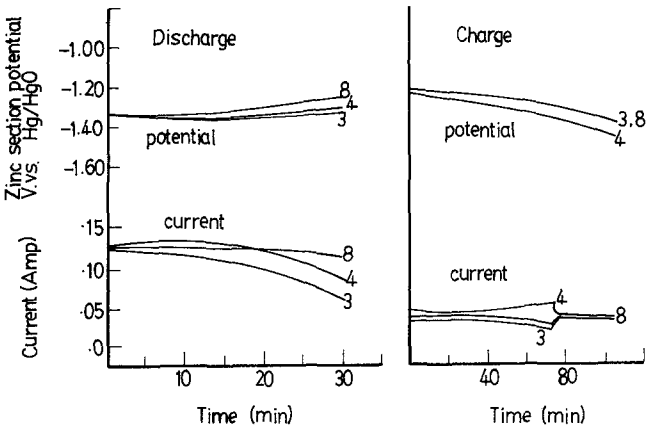

Fig. 13. Current and potential distribution of Sections 3, 4 and 8 of the zinc electrode for Cell 2 at Cycle 18.

the purpose of observing the influence of increasing the rate of charge and discharge on the current and potential distributions. The current and potential distributions during discharge in the later stages of cycling (Cycles 43–45), were fairly uniform except for the lower current on Section 1. The time period before the occurrence of rapid convergence of the current distribution on charging was further shortened. Towards the end of cycling (Cycles 55–57), Sections 1, 7 and the areas near the top edge had lower discharge currents than any of the other areas on the zinc electrode (as shown in Figs. 14–16). Also, the extent of non-uniformity in the current and potential distributions on the electrode increased.

3.3. *Shape change of zinc electrodes*

Figs. 17 and 18 show the zinc active material redistribution by weight per cent value versus section number plots together with sketches of shape change patterns which occurred on the zinc electrodes of Cells 1 and 2 after cycling. These shape change patterns were sketched from the observed shape change taking place at the electrodes. The areas inside the boundary curves indicate where the zinc active materials agglomerated. The thickness of these areas increased by as much as a factor of nearly 3 in some places (the original thickness of the uncycled zinc plates was 0·40 ± 0·04 mm; after cycling, the thickness of the areas inside the boundary curve increased to 0·40–1·10 mm). The areas between the boundary curves and the plate edges were nearly denuded of zinc active materials and the thickness of these areas decreased to that of the unpasted grid (0·22 mm) in some places.

In each of the weight per cent value versus section number plots, the horizontal broken line represents the average weight per cent value for all sections of the zinc plate before cycling. The solid discontinuous curve represents the weight per cent values of different sections of the zinc plate after cycling.

Although the number of test cycles carried out

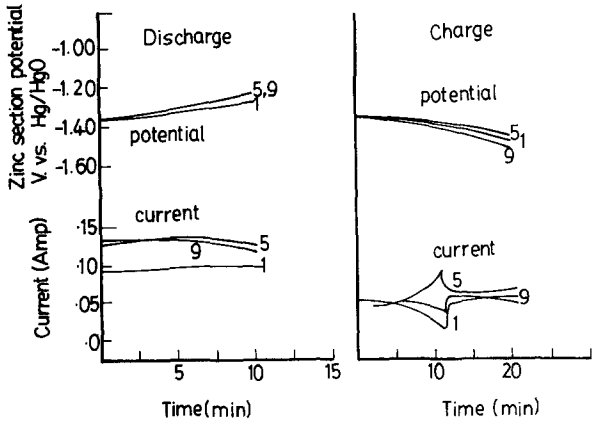

Fig. 14. Current and potential distribution of Sections 1, 5 and 9 of the zinc electrode for Cell 2 at Cycle 55.

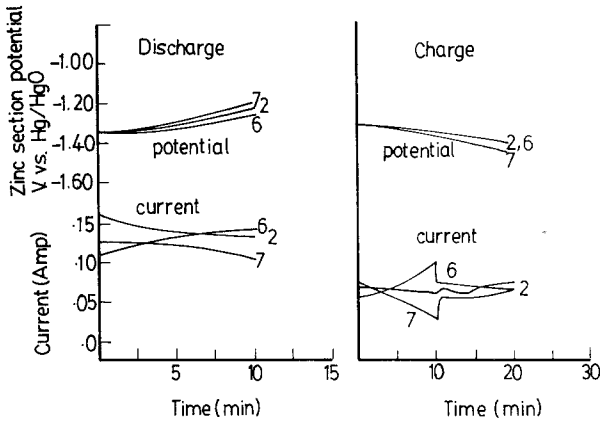

Fig. 15. Current and potential distribution of Sections 2, 6 and 7 of the zinc electrode for Cell 2 at Cycle 56.

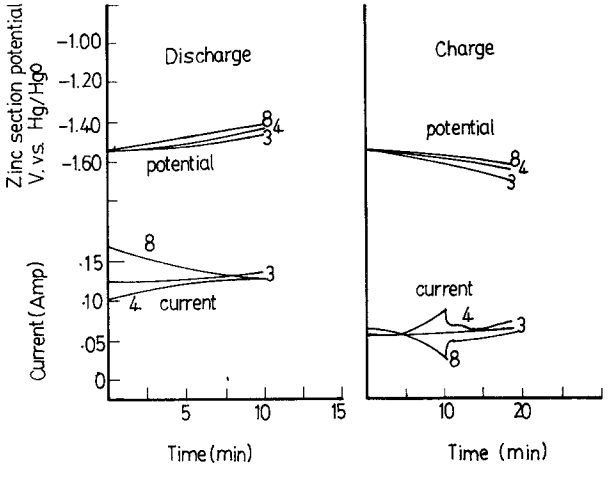

Fig. 16. Current and potential distribution of Sections 3, 4 and 8 of the zinc electrode for Cell 2 at Cycle 57.

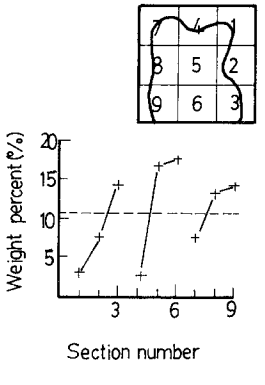

Fig. 17. The electrode shape change pattern and the weight per cent versus section number plot for the zinc electrode of Cell 1 after 36 cycles.

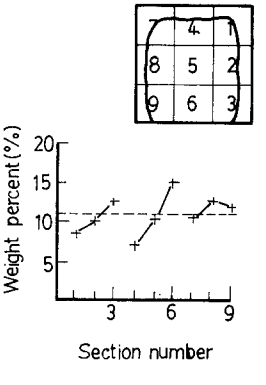

Fig. 18. The electrode shape change pattern and the weight per cent versus section number plot for the zinc electrode of Cell 2 after 57 cycles.

on Cell 2 was much larger than on Cell 1, and furthermore, Cell 2 was charged and discharged at a higher rate during the later stages of cycling, it can be observed from Figs. 17 and 18, that the extent of shape change of the zinc electrode of Cell 2 was much smaller than for the electrode of Cell 1. These results indicate clearly that the performance of Cell 2 over that of Cell 1 was significantly improved by adding to the edge sections of the separator systems of Cell 2 a layer of non-woven fabric treated with Fe_2O_3.

4. Discussion

Several trends and phenomena were observed from the results of current and potential distribution studies. During discharge, a large initial variation in current distribution was observed, after which the current distribution tended to converge gradually with time. During charge, the current distribution was uniform initially, diverged gradually with time, and then the current distribution on the electrode converged rapidly to a uniform value again when the cell was charged to a certain potential. The following analysis can explain some aspects of these characteristic trends and phenomena.

At the beginning of discharge, in an uncycled cell, there was a uniform distribution of zinc active material through the zinc electrode surface; the surface reaction overpotential could be neglected altogether, and the electrode was considered to have an equipotential surface. Therefore, the primary current distribution (which is determined by geometric factors) could be closely approached. This is the reason for the current distribution at the beginning of discharge being non-uniform and the current density highest at the edges of the electrode. When the discharge reaction proceeded, the extent of electrode polarization also increased with time due to the formation of the passive films caused by the decomposition of the zincate complex and the subsequent formation of oxide films within the pores and on the surface of the electrode [20–22]. When the electrode was polarized, the surface reaction overpotential could not be neglected and the electrode no longer approximated to an equipotential surface. The general effect of electrode polarization was to make the secondary current distribution more uniform than the primary current distribution, and the high current density at the edges of electrodes was eliminated. This can be regarded as the result of imposing an additional resistance at the electrode interface.

At the beginning of charging both current density and electrode polarization were high due to the decrease in electrode surface area resulting from the anodic dissolution during the previous discharge. This electrode polarization resulted in a secondary current distribution and it would explain the initial uniform current distribution on charging. As the charge reaction progressed, both current density and electrode polarization decreased with time due to the increase in electrode surface area resulting from the continuous deposition of zinc on the electrode. Thus the gradual divergence of the current distribution with time during charging can be explained. When the potential of the cell reached a higher value, the oxidation of Ag to Ag_2O occurring on the positive electrode changed to allow oxidation of Ag_2O to AgO. This shifting caused a rapid polarization of the electrode, which in turn brought about the observed rapid convergence of current distribution to uniformity.

The results also indicate that the performance of Cell 2 was significantly improved over that of Cell 1 by adding to the edge sections of the separator system of Cell 2 a layer of non-woven fabric treated with Fe_2O_3. This modification of the separator system has the effect of lowering the hydrogen overpotential and reducing the zinc plating efficiency on the edge sections of the zinc electrode. The charging efficiency on these sections was reduced because a portion of the charging current was consumed by gas production during charge. Although the apparent current on the edge sections was higher than that on the other parts of the electrode, the portion of current used on actual zinc deposition on the edge sections was smaller. Therefore, this modification can improve the uniformity of the zinc material distribution on the electrode surface in the early stages of cell cycling. This is the reason why the initiation of the electrode shape change was delayed and the extent of shape change occurring on the zinc electrode of Cell 2 was significantly reduced.

5. Conclusions

The non-uniformity of the current and potential

distributions on the zinc electrodes during cell cycling may be explained in terms of changes in the primary and secondary current distributions resulting from variations in electrode polarization.

The addition of a layer of non-woven fabric treated with Fe_2O_3 to the edge sections of the electrode has the effect of lowering the hydrogen overpotential and reducing the zinc plating efficiency on the edge sections of the zinc electrodes. This modification to the electrode separator system can improve the uniformity of the current and potential distributions, and improves the uniformity of the zinc material distribution on the electrode surface in the early stages of cell cycling.

Acknowledgement

This work was carried out with the financial assistance of the National Science Council of the Republic of China.

References

[1] S. P. Poa and C. H. Wu, *J. Appl. Electrochem.* 8 (1978) 427.
[2] J. W. Diggle, A. R. Despic, and J. O'M. Bockris, *J. Electrochem. Soc.* **115** (1968) 507.
[3] R. W. Powers, *Electrochem. Technol.* **5** (1967) 429.
[4] R. D. Naybour, *Electrochim. Acta* **13** (1968) 763.
[5] *Idem*, *J. Electrochem. Soc.* **116** (1969) 520.
[6] F. Mansfeld and S. Gilman, *ibid* **117** (1970) 588.
[7] *Idem*, *ibid* **117** (1970) 1154.
[8] *Idem*, *ibid* **117** (1970) 1328.
[9] *Idem*, *ibid* **117** (1970) 1521.
[10] M. W. Breiter, *Electrochim. Acta* **15** (1970) 1297.
[11] Z. Nagy and J. O'M. Bockris, *J. Electrochem. Soc.* **119** (1972) 1129.
[12] R. N. Elsdale, N. A. Hampson, P. C. Jones and A. N. Strachan, *J. Appl. Electrochem.* **1** (1971) 213.
[13] J. P. Elder, *J. Electrochem. Soc.* **116** (1969) 757.
[14] T. P. Dirkse, *ibid* **102** (1955) 9.
[15] T. P. Dirkse, D. Dewit, and R. Shoemaker, *ibid* **115** (1968) 422.
[16] M. Eisenberg, H. F. Bauman, and D. M. Brettner, *ibid* **108** (1961) 909.
[17] N. A. Hampson and M. J. Tarbox, *ibid* **110** (1963) 95.
[18] T. P. Dirkse and N. A. Hampson, *Electrochim. Acta* **16** (1971) 2049.
[19] J. McBreen, *J. Electrochem. Soc.* **119** (1972) 1620.
[20] R. W. Powers and M. W. Breiter, *ibid* **116** (1969) 719.
[21] R. W. Powers, *ibid* **116** (1969) 1652.
[22] M. N. Hull, J. E. Ellison, and J. E. Toni, *ibid* **117** (1970) 192.